DOI: 10.15480/882.9345

Eighth International Symposium on Marine Propulsors
smp'24, Berlin, Germany, March 2024

Numerical study of self-propulsion performance of a twin-screw cruise ship equipped with podded propellers

Jianhua Wang[1], Wentao Wang[2], Decheng Wan[1*]

[1] Computational Marine Hydrodynamics Lab (CMHL), School of Naval Architecture, Ocean and Civil Engineering, Shanghai Jiao Tong University, Shanghai, China
[2] China Ship Scientific Research Center (CSSRC), Wuxi, China
[*] Corresponding author: dcwan@sjtu.edu.cn

ABSTRACT

The interactions between a ship's hull and podded propulsors differ significantly from traditional hull-propeller interactions, leading to distinct influences on self-propulsion performance. In this study, we employed an in-house Computational Fluid Dynamics (CFD) solver, naoe-FOAM-SJTU, to predict the self-propulsion capabilities of a twin-screw cruise ship equipped with podded propulsors. Dynamic overset grid method is used to deal with the complex motions of ship hull-propeller system. The podded propulsor is simplified by introducing a gap between geometry of rotating propeller and pod for easy distribution of overset grids. Open water simulations were firstly conducted and compared with the experiment. Self-propulsion calculations were then carried out based on fully discretized approach and simulation results, such as thrust and torque, agree well with the available experimental data. Flow visualizations, such as pressure distribution on hull surface and podded propulsors, wake flow, vortical structures, etc. were presented and analyzed. The results showed that the present numerical approach is suitable and reliable in predicting the self-propulsion performance of ship self-propulsion with podded propellers.

Keywords

Ship self-propulsion, computational fluid dynamics, overset grid method, podded propellers, ship hull propeller interaction

1 INTRODUCTION

The podded propeller offers significant advantages in ship maneuverability due to its ability to rotate 360 degrees along the horizontal plane. Additionally, it aids in minimizing ship appendages such as propeller shafts and brackets, especially beneficial for twin-screw ships. Consequently, numerous newly manufactured vessels, particularly cruise ships, are being equipped with podded propellers. The dynamics between a ship's hull and podded propulsors differ notably from traditional hull-propeller interactions, exerting a distinct influence on self-propulsion performance. Hence, it is crucial to develop a suitable approach for assessing the hydrodynamic performance of ships employing podded propellers.

Numerical methods have been extensively employed to explore the performance of ship self-propulsion. Among these methods, the propeller body force model stands out as an efficient means to predict the hydrodynamic behavior of ship self-propulsion (Phillips et al. 2009, Feng et al. 2020, Wang et al. 2022). Despite its efficiency, accurately capturing intricate flow characteristics around rotating propellers remains a considerable challenge. This limitation poses difficulty in predicting the nuanced interactions between a ship's hull and podded propellers

In addition to the body force propeller model, the utilization of a fully discretized propeller through the dynamic overset grid method has proven successful in CFD simulations involving ship-propeller interaction. Carrica et al. (2010) demonstrated this by computing the self-propulsion of the KCS model, allowing for free trim and sinkage, utilizing a discretized propeller and achieving commendable agreement in their results. Similarly, Castro et al. (2011) performed simulations on the self-propulsion of the KCS model at full scale, employing a discretized propeller setup. Bekhit (2018) conducted simulations on JBC ship self-propulsion, comparing both body force propeller and fully discretized propeller models. The findings indicated that discretized propeller simulations provided a more comprehensive description of flow characteristics, while the body force model proved adequate for rapid predictions. Shen et al. (2015) integrated a dynamic overset grid module into the naoe-FOAM-SJTU solver and applied it to simulate KCS self-propulsion. Furthermore, Wang et al. (2019a) further employed the same approach to perform CFD investigations of self-propulsion for a twin-screw ship across various speeds.

Several studies have investigated the interactions between ship hulls and podded propellers. Zhao et al. (2019) utilized the sliding mesh technique to analyze the self-propulsion performance of a double L-type podded propeller. Huang et al. (2019) conducted a study on the

interactions between podded propulsors and cruise ship hulls using the commercial software STAR-CCM+, employing a sliding mesh to manage the rotating motion. Additionally, Wang et al. (2021) conducted RANS computations to assess ship self-propulsion, comparing a single-screw propeller with a hybrid contra-rotating podded propeller. Their findings revealed that podded propulsion exhibited higher efficiency compared to single-screw propulsion.

Numerous prior investigations into simulating podded propulsors have predominantly relied on commercial software employing the sliding mesh technique. However, this paper introduces a different approach by utilizing the in-house CFD solver with dynamic overset grid method to predict the hydrodynamic performance of a cruise ship equipped with twin podded propulsors. The main objective for the present study is to find an appropriate numerical approach to predict ship self-propulsion with podded propellers. The paper is structured as follows: firstly, it outlines the numerical approach, encompassing the viscous flow solver and the overset grid method. Subsequently, it delves into the geometry model and numerical setup. Following this, the paper presents and discusses the numerical results, including open water calculations, towing conditions of the bare hull, and self-propulsion scenarios. Lastly, the study concludes by summarizing the findings obtained in this investigation.

2 NUMERICAL APPROACHES

2.1 CFD Solver

The present simulations rely on the in-house CFD solver, naoe-FOAM-SJTU, as introduced by Wang et al. (2019b). This solver has been specifically developed to handle complex marine hydrodynamic problems. Notably, the naoe-FOAM-SJTU solver has featured modules including the dynamic overset grid and 6DoF motion module with a hierarchy of bodies. This unique feature allows the convenient use of direct simulations of ship self-propulsion with rotating propellers. The naoe-FOAM-SJTU solver has gained substantial expertise in addressing various ship hydrodynamic challenges in recent years. These include investigations into ship resistance (Zha et al 2015), self-propulsion (Shen et al 2015), maneuvering capabilities (Wang and Wan, 2018; 2020), as well as seakeeping performance (Shen and Wan, 2013; 2016).

The naoe-FOAM-SJTU solver employs the computation of Reynolds-Averaged Navier-Stokes (RANS) equations for unsteady, incompressible, and immiscible two-phase flows. Turbulence is modelled with the standard shear stress (SST) k-ω two-equation model (Menter et al., 2003). Wall functions are used in the near wall region. To accurately represent the free surface, the solver utilizes an algebraic Volume of Fluid (VOF) method integrated with the artificial compression technique developed by Berberović et al. (2009) and implemented within OpenFOAM.

2.2 Overset Grid Technique

The successful application of the discretized propeller model hinges on effectively managing the grid motion of rotating propellers. The naoe-FOAM-SJTU solver incorporates dynamic overset grid capabilities along with a 6DoF motion solver equipped with a hierarchical structure of bodies. Each overset mesh within the solver operates independently, enabling unrestricted movement for every mesh component. This feature facilitates the direct simulation of ship self-propulsion, specifically involving rotating propellers. Figure 1 illustrates the distribution of the overset grid around rotating propellers, delineating the rotating segment in red and the fixed segment in blue. For a comprehensive understanding of the overset grid module's implementation in OpenFOAM, readers can refer to Shen et al. (2015). In this particular study, the geometries have been deconstructed into several overlapping grids. This approach allows for the direct simulation of ship self-propulsion, specifically considering podded propulsors.

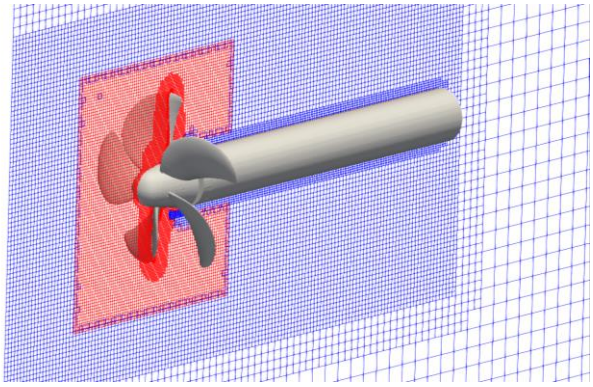

Figure 1 Overset grid distribution

3 GEOMETRY AND NUMERICAL SETUP

3.1 Geometry Model

The simulations for ship self-propulsion in this study feature a cruise ship equipped with twin podded propulsors. The 3D geometry model depicting the cruise ship is displayed in Figure 2, while Table 1 provides the main particulars of the vessel. The ship model measures 7.555 meters in length, and each podded propulsor incorporates a five-blade propeller, with detailed specifications outlined in Table 2.

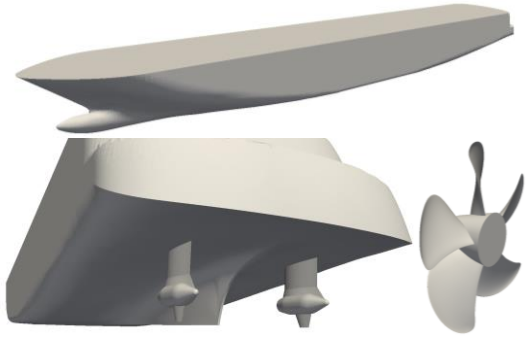

Figure 2 Geometry model of cruise ship and podded propulsor

Table 1. Main particulars of cruise ship model

Main particulars	symbol	Model scale
Scale factor	λ	38
Length between perpendiculars	L_{pp}(m)	7.555
Beam of waterline	B_{wL}(m)	0.979
Draft	T(m)	0.217
Displacement	Δ (m^2)	1.192
Block coefficient	C_B(m)	0.739
Longitudinal center of buoyancy, fwd+	LCB(%L_{PP})	-1.724
Vertical center of gravity (from keel)	KG(m)	0.258
Number of propellers	I_{zz}/L_{pp}	2

Table 2. Main particulars of propeller model

Main particulars	symbol	Model scale
Scale factor	λ	38
Diameter	D(m)	0.15
Pitch ratio	$P_{0.7}/D$	1.15
Area ratio	A_e/A_0	0.62
Number of blades	Z	5
Rotation	-	Inward

3.2 Numerical Setup

For the direct simulation of self-propulsion, the computational domain consists of three-part grids: the hull grid, propeller grid, and background grid. However, in simulations involving open water and bare hull towing, a two-part grid configuration is utilized. Figure 3 illustrates the domain of overset regions employed in the current simulation setup.

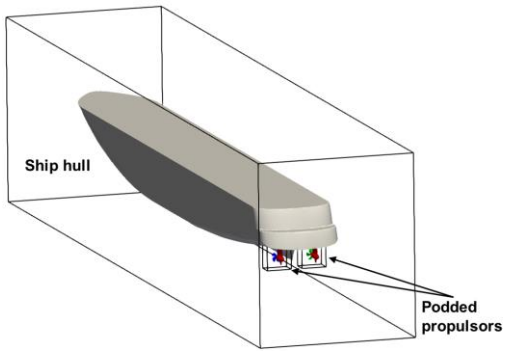

Figure 3 Overset regions of ship hull and podded propulsors

To adequately resolve propeller revolutions per second (RPS), a time step of $\Delta t = 4\times10^{-4} s$ is employed in the computations. All computations are executed at the High-Performance Computing (HPC) facility in SJTU. Each node comprises 2 CPUs with 20 cores per node and 64GB accessible memory (Intel Xeon E5-2680v2 @2.8 GHz). Specifically, 40 processors are dedicated to calculating the ship self-propulsion simulation.

The predicted data for both the open water and self-propulsion cases are presented using non-dimensional values, as outlined below.

$$J = \frac{V}{nD} \tag{1}$$

$$K_{Tp} = \frac{T_p}{\rho n^2 D^4} \tag{2}$$

$$K_{Tu} = \frac{T_u}{\rho n^2 D^4} \tag{3}$$

$$K_Q = \frac{Q}{\rho n^2 D^5} \tag{4}$$

$$\eta_0 = \frac{J}{2\pi}\cdot\frac{K_{Tu}}{K_Q} \tag{5}$$

where J represents the advance ratio, K_{Tu} denotes the thrust coefficient of the unit, K_{Tp} signifies the thrust coefficient of the propeller, K_Q stands for the torque coefficient and η_0 is open water efficiency.

It should be noted that all the data presented in the following study is in model scale.

4 RESULTS AND DISCUSSIONS

4.1 Open Water Test

To begin, numerical simulations replicating the open water test for a single podded propeller are performed. The simulation conditions mirror those of the experiments conducted in the towing tank. In this simulation, the propeller advances with a fixed revolutions per second (RPS=11.39r/s), while the towing speed varies to predict the propulsion performance. Figure 4 displays the computational domain for the open water test. Specifically, only the rotating propeller is segmented into a moving part within an overset grid arrangement. For clarity, Figure 5 illustrates the computational grid surrounding the podded propulsor, where the red color demarcates the rotating region.

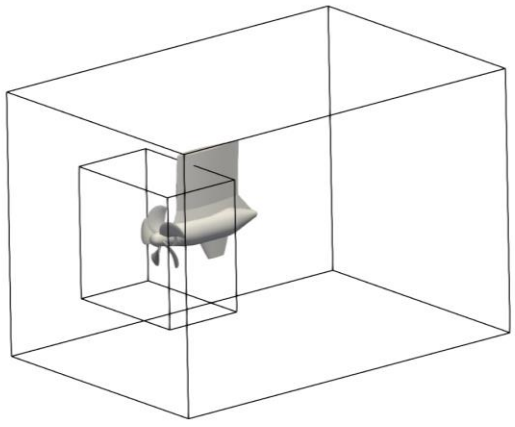

Figure 4 Computational domain of open water test

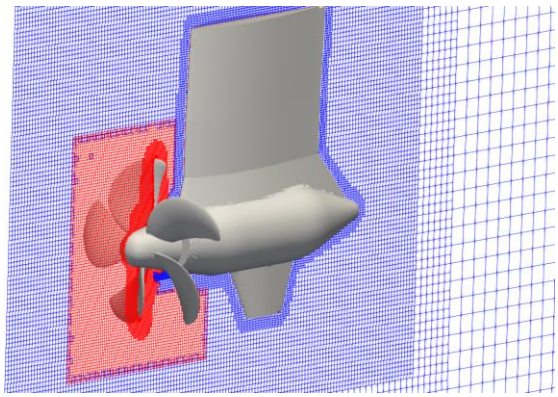

Figure 5 Overset grid distribution around podded propulsor

Simulations for nine cases covering a range of J values from 0.1 to 0.9 were carried out. The predicted propulsion coefficients, K_{Tp}, K_Q, and efficiency η_0 (as displayed in Figure 6), were systematically compared with the corresponding experimental data. The computational error for the design case (J=0.9) is about 5.3%. The results indicate that our current overset grid approach yields promising predictions for the open water tests. The unit thrust is a little smaller than that of the propeller thrust. For the design case, K_{Tu} is 0.174 and K_{Tp} is 0.201. These outcomes establish a solid foundation for subsequent self-propulsion simulations.

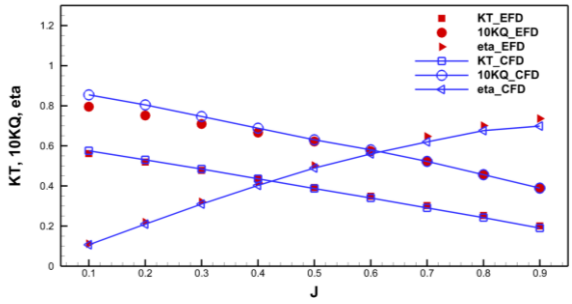

Figure 6 Comparison of open water data with experiment

4.2 Towing Test

Before proceeding with the simulation of the self-propulsion case, we performed towing tests for the bare hull. Figure 7 depicts the computational domain employed for the towing test of the cruise ship. The computational region spans as follows: $-L_{pp} \leq x \leq 3L_{pp}$, $-L_{pp} \leq y \leq L_{pp}$, $-L_{pp} \leq z \leq 0.5L_{pp}$. Three distinct ship speeds, namely 17 knots, 20 knots, and 23 knots (corresponding to Fr=0.165, 0.194, 0.223), were selected to predict the ship's resistance.

The predicted ship resistance in model scale is presented in Figure 8, illustrating convergence within approximately 20 seconds of simulation time. A comparison between the predicted resistance (mean value from 10s-20s) and experimental data is tabulated in Table 3. Notably, our present results exhibit a high level of agreement with the towing tank test, displaying an error rate lower than 3%.

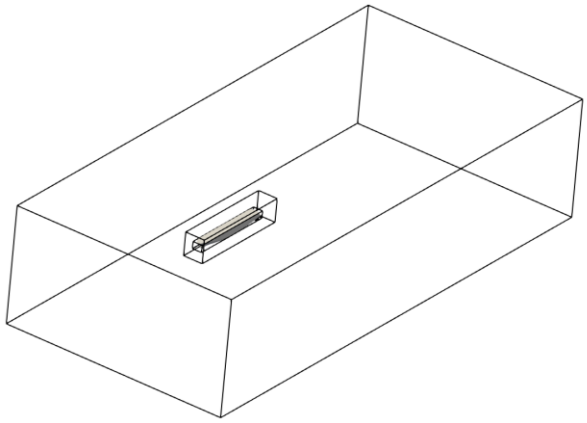

Figure 7 Computational domain for towing test

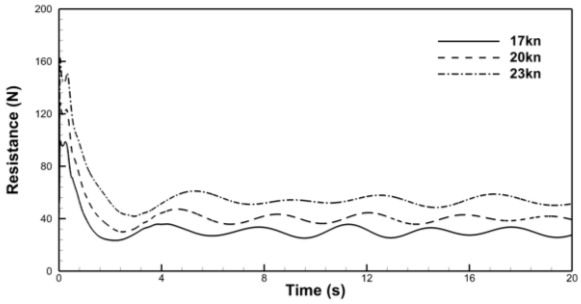

Figure 8 Time history of ship resistance under different speeds

Table 3. Comparison of ship resistance in model scale with experimental data

Speed (kn)	EFD (N)	CFD (N)	Error
17	29.655	30.115	1.55%
20	40.261	40.184	-0.19%
23	55.721	54.121	-2.87%

Figure 9 displays the wave patterns corresponding to different ship speeds. Notably, the Kelvin wave is distinctly evident, with higher wave elevations observed at greater ship speeds. The accurate prediction achieved in the towing test sets a solid groundwork for the subsequent self-propulsion simulation. Leveraging the steady state attained from the towing case will be instrumental in mapping it to the self-propulsion scenario, thereby expediting the convergence of the flow field.

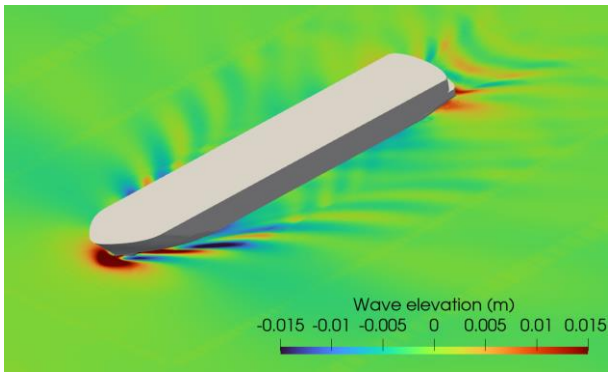

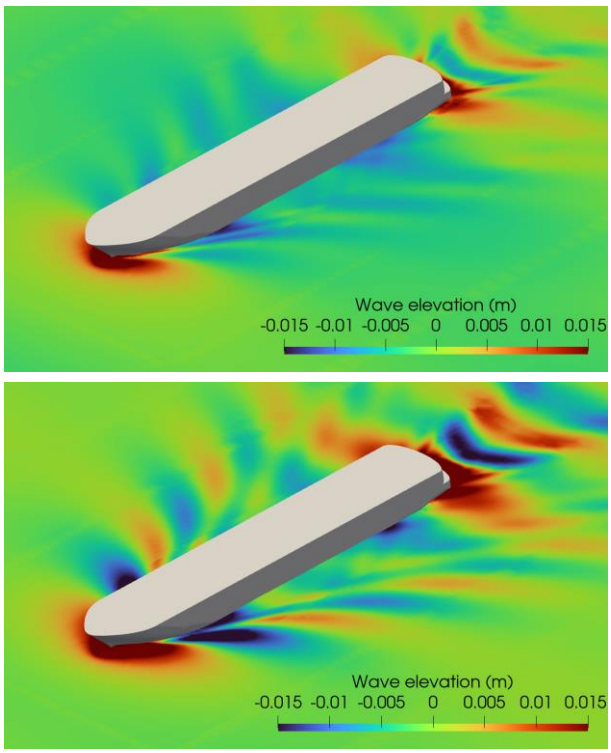

Figure 9 Wave pattern at different ship speeds (up:17kn, mid: 20kn, down: 23kn)

4.3 Self-propulsion Test

The self-propulsion simulation closely aligns with the experimental test conducted in the towing tank. To simulate this scenario, the computational grid is divided into four parts, comprising one for the background, one dedicated to the ship hull, and two segments for the rotating propellers. Figure 10 depicts the overset grid distribution surrounding the ship hull and the twin podded propellers. The total grid count amounts to 7.8 million.

It should be noted that the present calculations apply wall functions near wall and the y+ value for hull grid and propeller grid are around 60 and 80, respectively.

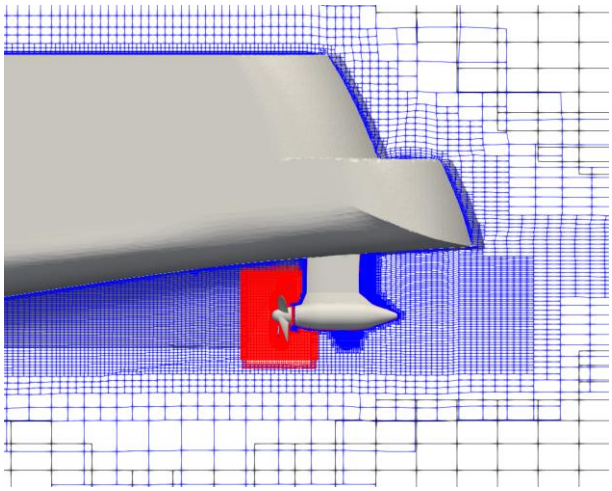

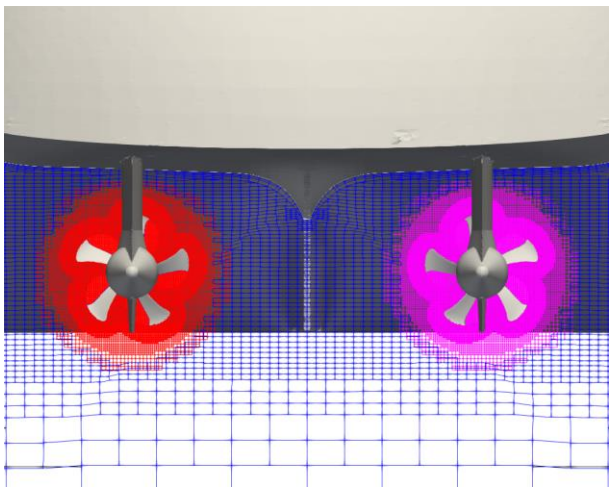

Figure 10 Overset grid distribution around twin podded propellers (up: profile view, down: transverse view)

Throughout the simulation process, the revolutions per second (RPS) remained fixed, correlating with the experimental values. According to the self-propulsion test, the ship self-propulsion point is obtained using the interpolation approach and the RPS for 17kn, 20kn and 23kn are 9.706, 11.39 and 13.357, respectively. Table 4 outlines the predicted propeller thrust (total thrust of twin propellers) at various ship speeds. The simulation results exhibit a relatively good agreement with experimental measurements. Discrepancies observed might stem from variations in experimental conditions and the CFD setup. Notably, most CFD simulation studies on self-propulsion employ a PI controller to ascertain the self-propulsion point and subsequently fix the RPS derived from CFD. Further computational investigations will be conducted to evaluate whether these discrepancies influence the accuracy of thrust predictions.

Table 4. Comparison of propeller total thrust with experiment

Speed (kn)	RPS (r/s)	EFD (N)	CFD (N)	Error
17	9.706	16.69	15.152	-9.21%
20	11.39	23.01	20.536	-10.75%
23	13.357	33.45	29.686	-11.25%

To investigate the hydrodynamic performance of the podded propulsor behind the ship hull, the time histories of single propeller thrust at various ship speeds are depicted in Figure 11. Noticeably, thrust values significantly increase with higher ship speeds. Moreover, distinct high-frequency oscillations are evident, featuring several major frequencies. To delve deeper into the underlying cause of these high-frequency oscillations, frequency domain results obtained through Fourier transform are presented in Figure 12. Table 5 provides the results of the three major frequencies derived from the FFT transform.

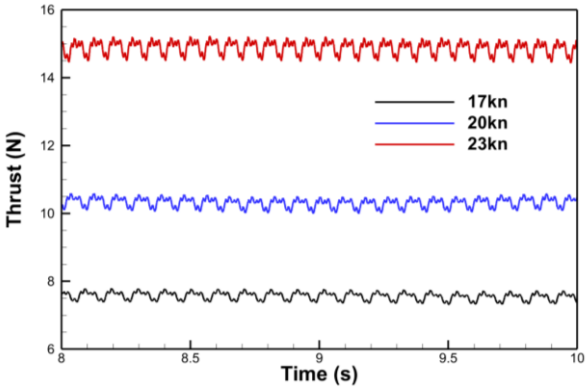

Figure 11 Comparison of the time histories of single propeller (port side) thrust at different speeds

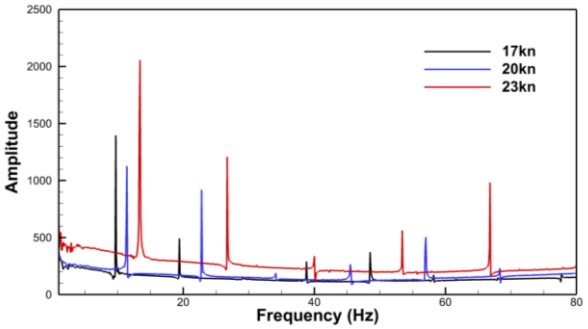

Figure 12 Comparison of FFT results for propeller thrust at different speeds

The analysis of Figure 12 and Table 5 reveals distinct characteristics in the identified frequencies. HF1 aligns with the propeller RPS frequency, indicating its direct association with propeller rotation. The frequency HF2 is precisely twice that of HF1, primarily stemming from the pod's profile. While the pod configuration is symmetrical from the port side to the starboard side, substantial differences exist between the top and bottom sections. Consequently, after each 180° rotation of the propeller, the interference behind the pod varies, resulting in the observed frequency doubling oscillation. Furthermore, high frequency 3 corresponds to five times the propeller rotation frequency, primarily attributed to the current podded propeller employing a 5-blade configuration. These comprehensive numerical findings highlight the CFD approach's capability in capturing the transient hydrodynamic characteristics of the aft pod propeller. This data proves invaluable for studying the hydrodynamic performance and interaction between the ship hull and podded propeller.

Table 5. Comparison of major frequencies at different speeds

Speed (kn)	HF1 (Hz)	HF2 (Hz)	HF3 (Hz)	RPS (r/s)
17	9.735	19.372	48.491	9.706
20	11.332	22.845	56.991	11.39
23	13.403	26.683	66.832	13.357

Figure 13 showcases the comparison of wake flow distribution around twin podded propellers, depicting the wake fraction (*w*) and also colored by *w*. Notably, the primary features remain consistent across different scenarios, although the wake region notably expands in cases with higher speeds. An observed effect is the flow acceleration induced by the propeller rotation.

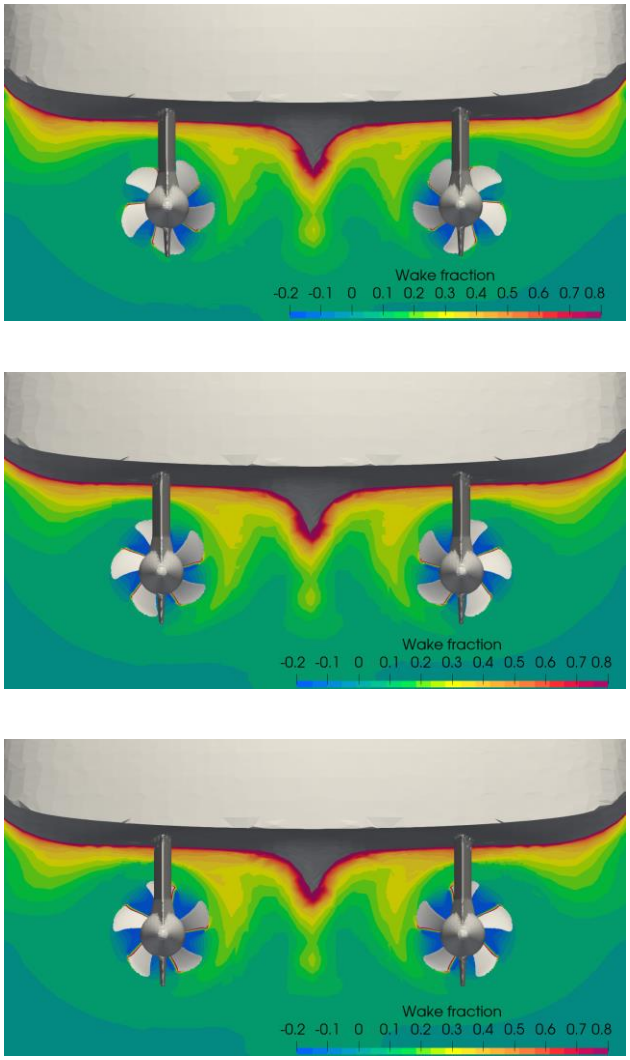

Figure 13 Comparison of wake flow at different ship speeds (up:17kn, mid: 20kn, down: 23kn)

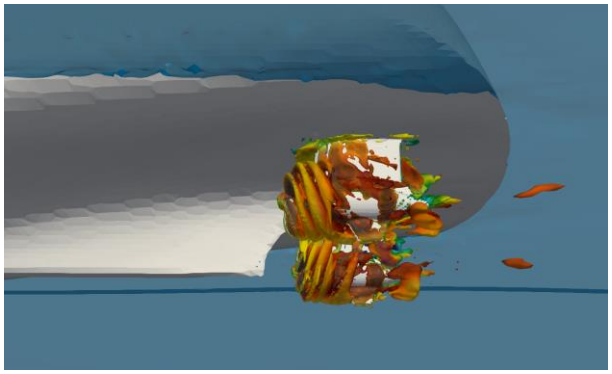

Figure 14 Vortical structures around podded propulsors

Figure 14 illustrates the 3D vortical structures surrounding the twin podded propellers. Notably, the powerful tip vortices experience disruption caused by the aligned pod structure. Additionally, discernible necklace vortices emerge at the junction between the ship hull and the pod. Interestingly, an observed asymmetry between the inner and outer parts of these vortices offers insight into explaining the occurrence of HF2 as documented in Figure 12 and Table 5.

5 CONCLUSIONS

This paper employs the dynamic overset grid technique to predict the hydrodynamic interaction between a cruise ship hull and twin podded propulsors. The study's predictions for the propulsion coefficient in the open water case and the ship's resistance during towing align well with experimental outcomes. In the self-propulsion analysis, three ship speeds are examined, employing fixed RPS values corresponding to experimental data. The predicted thrust of the podded propulsor is validated through comparison with measured data. Notably, the CFD simulations reveal several high-frequency features, whose origins are associated with the propeller's rotation rate as observed in the FFT results of thrust. Detailed presentations of wake distribution and vortical structures offer insights into the hydrodynamic behaviors inherent in ship self-propulsion featuring podded propellers.

Future work will focus on more validation study, including grid convergence study and the simulation based on self-propulsion point obtained by the CFD result. In addition, more work will be done for the detailed analysis on the hull-propeller interaction factors.

ACKNOWLEDGMENTS

This work is supported by National Natural Science Foundation of China (52131102), to which the authors are most grateful.

REFERENCES

Bekhit, A. S. (2018). "Numerical simulation of the ship self-propulsion prediction using body force method and fully discretized propeller model," IOP Conference Series: Materials Science and Engineering, **400**, 042004.

Berberović, E., van Hinsberg, N. P., Jakirlić, S., Roisman, I. V., & Tropea, C. (2009). "Drop impact onto a liquid layer of finite thickness: Dynamics of the cavity evolution," Physical Review E, **79(3)**, 036306.

Carrica, P. M., Castro, A. M., & Stern, F. (2010). "Self-propulsion computations using a speed controller and a discretized propeller with dynamic overset grids," Journal of Marine Science Technology, **15(4)**, 316–330.

Castro, A. M., Carrica, P. M., & Stern, F. (2011). "Full scale self-propulsion computations using discretized propeller for the KRISO container ship KCS," Computers & Fluids, **51(1)**, 35–47.

Feng, D., Yu, J., He, R., Zhang, Z., & Wang, X. (2020). "Improved body force propulsion model for ship propeller simulation," Applied Ocean Research, **104**, 102328.

Huang, Y. M., Yang, Y. F., He, W., & Wang, T. T. (2019). "Numerical Prediction of Pressure Fluctuations on Cruise Ship Hull Induced by Podded Propulsors," Proceedings of the International Ocean and Polar Engineering Conference. ISOPE-I-19-620.

Menter, F. R., Kuntz, M., & Langtry, R. (2003). "Ten years of industrial experience with the SST turbulence model," Turbulence, Heat and Mass Transfer, **4(1)**, 625-632.

Phillips, A. B., Turnock, S. R., Furlong, M. (2009). "Evaluation of manoeuvring coefficients of a self-propelled ship using a blade element momentum propeller model coupled to a Reynolds averaged Navier Stokes flow solver," Ocean Engineering, **36(15–16)**, 1217–1225.

Shen, Z., & Wan, D. C. (2013). "RANS computations of added resistance and motions of a ship in head waves," International Journal of Offshore and Polar Engineering, **23(04)**, 264-271.

Shen, Z., Wan, D. C., & Carrica, P. M. (2015). "Dynamic overset grids in OpenFOAM with application to KCS self-propulsion and maneuvering," Ocean Engineering, **108**, 287–306.

Shen, Z. R., & Wan, D. C. (2016). "An irregular wave generating approach based on naoe-FOAM-SJTU solver," China Ocean Engineering, **30**, 177-192.

Wang, J., & Wan, D. (2018). "CFD investigations of ship maneuvering in waves using naoe-FOAM-SJTU Solver," Journal of Marine Science and Application, **17(3)**, 443-458.

Wang, J., & Wan, D. (2020). "CFD study of ship stopping maneuver by overset grid technique," Ocean Engineering, **197**, 106895.

Wang, J., Zhao, W., & Wan, D. C. (2019a). "Simulations of Self-Propelled Fully Appended Ship Model at Different Speeds," International Journal of Computational Methods, **16(3)**, 1840015.

Wang, J., Zhao, W. W., & Wan, D. C. (2019b). "Development of naoe-FOAM-SJTU solver based on OpenFOAM for marine hydrodynamics," Journal of Hydrodynamics, **31**, 1-20.

Wang, M., Wan, D. C., & Wang, J. (2022). "An improved BEMT model based on agent actuating disk with application to ship self-propulsion simulation," Ocean Engineering, **266**, 112787.

Wang, Z. Z., Min, S. S., Peng, F., & Shen, X. R. (2021). "Comparison of self-propulsion performance between vessels with single-screw propulsion and hybrid contra-rotating podded propulsion," Ocean Engineering, **232**, 109095.

Zha, R. S., Ye, H. X., Shen, Z. R., & Wan, D. C. (2015). "Numerical computations of resistance of high speed catamaran in calm water," Journal of Hydrodynamics, **26(6)**, 930-938.

Zhao, D., Guo, C., Lin, J., Zhang, Z., & Bai, X. (2019). "Prediction of self-propulsion performance of ship model with double L-type podded propulsors and conversion method for full-scale ship," Journal of Marine Science and Engineering, **7(5)**, 162.